J. Fluid Mech. (1984), *vol.* 145, *pp.* 423–445
Printed in Great Britain

An experimental study of the response of nearly isotropic turbulence to a spectrally local disturbance

By ERIC C. ITSWEIRE AND CHARLES W. VAN ATTA
Department of Applied Mechanics and Engineering Sciences, University of California, San Diego, La Jolla, CA 92093

(Received 28 July 1983 and in revised form 9 April 1984)

A grid-generated, nearly isotropic turbulent flow was subjected to a spectrally local disturbance whose scale was close to but larger than the Kolmogorov scale. A nearly sinusoidal ripple in the velocity was introduced by placing a low-solidity screen of very fine wires (called a 'zither' by Kellogg & Corrsin 1980) downstream of a classical biplane grid. Measurements of the fluctuating velocity components normal to the screen wires show strong spatial oscillations of the second-order moments. Close to the screen the flow is quite inhomogeneous and anisotropic, but relaxes toward isotropy. After a short period of initial growth, the longitudinal one-dimensional spectrum $E_{11}(k_1)$ exhibits an unusual decay behaviour, especially after the Reynolds stress created by the mean shear of the boundary layers and 'laminar' wakes of the screen wires has vanished. Bispectra and one-dimensional transfer terms do not show evidence of any preferred interaction between longitudinal wavenumbers, but an increased energy transfer to large wavenumbers is observed at small x_1/d. The resulting increase of energy in the high-wavenumber end of the spectra is consistent with results of Townsend (1951). An energy budget downstream of the zither shows that the pressure–velocity correlations are important in the nonlinear interactions.

1. Introduction

In recent years the development of new experimental techniques such as conditional sampling, image processing and phase averaging combined with flow visualization has given useful insight into the mixing processes of inhomogeneous turbulent shear flows by retaining information of their time-dependent characteristics. But, for homogeneous turbulent flows in which organized motions are not clearly defined, the most useful approach for examining kinetic energy and scalar transfer is to study the dynamics of the flow through the evolution of the mean moments, as is done in statistical mechanics.

Until now, numerical modelling of nearly homogeneous turbulence has not produced much insight in understanding the interaction between different wavenumbers. The development of a new generation of computers has allowed a direct simulation of low-to-moderate Reynolds-number flows and should enhance the study of their response to spectrally local disturbances, although the relatively small range of computational scales available restricts simulation of the dynamics of local energy transfer to low Reynolds number. The present relatively low-Reynolds-number experiment was undertaken to examine the behaviour of local wavenumber interactions and to provide motivation and comparison data for comparable direct numerical simulation and model calculations.

Recently published experimental results of earlier work by Kellogg & Corrsin (1965, 1980) studied the evolution of a spectrally local disturbance in grid-generated nearly isotropic turbulence. In this initial experimental attack on the problem of narrow-band spectral transfer of energy in turbulence, they invented a useful device (a 'zither') for producing a narrow-band disturbance in wavenumber whose evolution and interaction with other wavenumber components could be studied experimentally. Other workers (e.g. Warhaft & Lumley 1978; Srcenivasan *et al.* 1980; Sirivat & Warhaft 1983), have used heated low-solidity screens in isotropic turbulence to generate temperature fluctuations, but were not interested in the evolution of the velocity disturbance near the screens. The disturbance, which consists of a narrow plane slab in wavenumber space, is not ideal for comparison with published theoretical results and introduces a non-negligible amount of energy. The ideal perturbations that have been studied theoretically contain a small fraction of the total energy in a small spherical shell (e.g. Kraichnan 1959). Direct numerical simulations allow the possibility of tailoring the initial disturbance to the experimentally realizable case and to other non-ideal disturbances arising in practical applications. In the present work, Kellogg & Corrsin's measurements have been extended by using two X-wire probes instead of two single-wire probes. The second-order moment measurements show that the departure of the disturbed turbulence from the initial isotropic state is due mainly to the production of kinetic energy by the Reynolds stress and the local mean gradients created by the zither. In order to determine the relative strength of wavenumber interactions, which involve three given wavenumbers, it is necessary to evaluate third-order spectral terms known as bispectra. An approach developed by Lii, Rosenblatt & Van Atta (1976) and Helland, Lii & Rosenblatt (1978) is limited by the experimental difficulty of measuring all of the relevant bispectral terms required to compute the net spectral energy transfer. A second approach developed by Wilson (1974) and extended by Van Atta (1979*a*) decomposes the velocity field in terms of discrete orthogonal Fourier modes and should be more suitable to this case, since the perturbation introduced by the zither can be considered as being a single Fourier mode once the wakes of the zither wires have merged. The results of the latter approach yield a straightforward interpretation in terms of local spectral energy transfer in terms of quantities readily accessible in a direct simulation or model calculation (e.g. Herring 1980).

2. Experimental design

The experiments were conducted in the low-speed low-turbulence wind tunnel in the Department of Applied Mechanics and Engineering Sciences of the University of California, San Diego. This tunnel, which has been previously described by Helland, Lii & Rosenblatt (1977, 1979), has a test section 76 cm × 76 cm that is 9 m long. A biplane grid of round polished dural rods was located 2.4 m from the end of the contraction section. The grid mesh length was $M = 5.08$ cm and the diameter of the rods was 0.953 cm, giving a solidity $\sigma_G = 32\,\%$. Downstream of the grid, the 'zither', which consists of an array of fine vertical wires, was introduced at $x_{1z}/M = 40$ as shown in figure 1. The zither was made of stainless-steel music wires of diameter $d = 76.2$ μm, equally spaced by a distance $m = 1.625$ mm. The solidity of the screen was $\sigma_z = 4.76\,\%$. To allow accurate positioning of the probes relative to the plane of the screen, the zither was mounted in a frame attached to a small Plexiglas section equipped with the traversing mechanism. The wind tunnel was run in closed-loop configuration to reduce dust accumulation on the zither wires. For

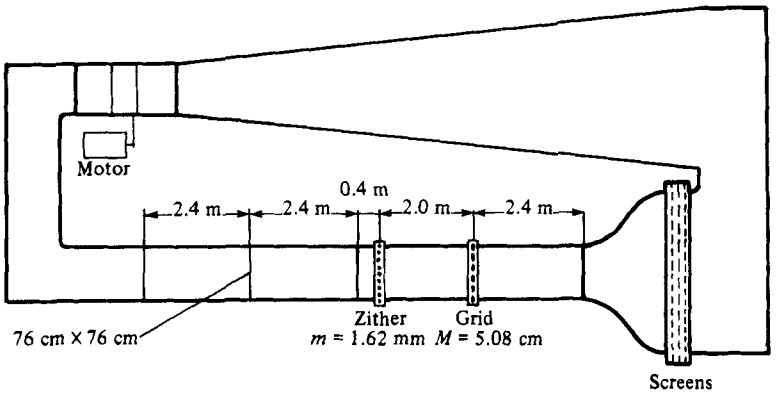

FIGURE 1. Wind-tunnel set-up.

running times of several hours, the increase in temperature was a few tenths of a degree. The traversing mechanism especially built for this experiment consisted of an airfoil-shaped aluminium profile cross-member 1 cm thick resting on rails on both sides of the Plexiglas section. The interior of the airfoil was machined to receive two dovetail-shaped slugs providing the transversal motion of the probes through threaded rods. For hot-wire calibrations, both slugs allowed rotation of the probe holders around a vertical axis from $-10°$ to $+10°$ in steps of $1° \pm 0.1°$. All fittings were made tight to eliminate possible vibrations, and no vibrations were observed. Each probe holder was equipped with a fine adjustment to achieve accurate longitudinal positioning of both probes.

3. Measurements

Simultaneous two-point measurements of the longitudinal and transversal components of the velocity field were made using two X-wire probes. The probes were miniature X-wire DISA 55P61. A small yaw angle with respect to the free-stream velocity was used to enable establishing a very small probe separation with minimum support interaction. The hot wires were made of 5 μm diameter platinum–tungsten wire 1 mm long. The sensing length in the transversal direction was 0.7 mm, which is equal to half the wavelength of the disturbance. The hot wires were operated at an overheat of 50 % by DISA 55M01 constant-temperature anemometers. The output of each anemometer was connected to a buck-and-gain amplifier before recording on a Honeywell 7600 FM analog recorder at a tape speed of 19 cm/s. The anemometer signals were not linearized before recording. Later, the analog signals were low-pass filtered and digitized on a 14-bit A/D converter. The sample rate, the number of samples and the number of records are given in table 1. Most of the data reduction was performed on a CDC 7600 located at Lawrence Berkeley Laboratory, but some was done at UCSD on the laboratory DEC 11/23 microcomputer.

The mean flow was monitored by a Pitot tube connected to a Baratron MKS 3 mm head pressure transducer. The temperature of the flow was measured by a platinum resistance thermometer system and kept constant within ± 0.2 °C. The X-wire calibrations were performed with the grid and zither removed from the tunnel using 54 measurement points at different speeds and pitch angles both before and after each set of measurements. First for each wire the coefficients from a modified King's law

Experiment	Filtering frequency (Hz)	Sample rate (Hz)	Number of samples/channel	Number of records
Longitudinal decay	3500	7000	4096	150
Transversal profiles	3000	6000	2048	100

TABLE 1. Sampling parameters

(Collis & Williams 1959) were determined using a least-squares fit to 'linearize' the anemometer signals:

$$E_{bi}^2 = A_i + B_i U^{0.45},$$

where E_{bi} is the bridge voltage. The 'linearized voltage' is them defined as:

$$E_{\ell i} = \left(\frac{E_{bi}^2 - A}{B}\right)^{2.22} \quad \text{in m/s.}$$

The conversion equations for the two velocity components (where a, b, and c were obtained by regression) are

$$U = a_1 + b_1 E_{\ell 1} + c_1 E_{\ell 2},$$
$$V = a_1' + b_1' E_{\ell 1} + c_1' E_{\ell 2}.$$

The wind tunnel was operated at a mean speed of $U = 6.5$ m/s. The measured turbulent intensities were consistent with earlier measurements by Chen (1969). The main characteristics of the incoming turbulent flow approaching the zither are given in table 2. The spacing between adjacent zither wires was $m = 1.625$ mm, providing ratios between m, the Taylor microscale λ and the Kolmogorov scale η:

$$\lambda > m > \eta,$$

$$\frac{m}{\lambda} = 0.31, \quad \frac{m}{\eta} = 3.4.$$

Ideally, the scale separation should be larger, especially between m and η. One way to achieve this might be to operate at a higher Reynolds number by substantially increasing the mean speed $\bar{U}_\infty$, but the Reynolds number of each individual zither wire would eventually increase to a point where vortex shedding occurs. Under the present experimental conditions we have no vortex shedding with

$$R_w = \frac{\bar{U}_\infty d}{\nu} \sim 32.$$

In a preliminary experiment no vortex shedding was observed for a wire Reynolds number as high as the Kármán critical value of 40. This is consistent with observations reported by Warhaft (1980). To avoid vortex shedding at higher speeds, one could reduce the diameter of the zither wires. An attempt was made to use a smaller diameter $d = 51$ μm, but most of the wires broke when put under the tension necessary to prevent bowing and vibrations under the prevailing dynamic conditions. Other advantages in decreasing d are a reduced energy input and a more localized disturbance.

$\bar{U}_\infty = 6.3$ m/s	$x/m = 40$
$\bar{\epsilon} \approx 760$ cm^2/s^3	$\langle u^2\rangle^{\frac{1}{2}}/\bar{U}_\infty = 1.65\,\%$
$R_G = \bar{U}M/\nu = 22400$	$\langle v^2\rangle^{\frac{1}{2}}/\bar{U}_\infty = 1.43\,\%$
$R_\lambda = \langle u^2\rangle^{\frac{1}{2}}\lambda/\nu = 32$	$M = 5.08$ cm
$\eta \approx 0.047$ cm	$\lambda = 0.53$ cm

TABLE 2. Characteristics of the incoming turbulence; λ is the 'transversal' Taylor microscale, ϵ the dissipation rate and ν the Kolmogorov microscale

4. Space–time characteristics of the disturbance

The turbulence is assumed to be homogeneous in the vertical (x_3) direction along the length of the zither wires. Some exploratory measurements of w by Kellogg (1965) show evidence that, even though the turbulence is three-dimensional, most of the energy transfer due to the zither occurs between u and v by interaction of wavenumbers located in the (x_1, x_2)-plane. This was attributed to the two-dimensional nature of the disturbance.

The evolution of the mean profiles $\bar{U}$ and $\bar{V}$ for different x_1/d shown in figure 2 confirms the periodic nature of the disturbance. By choice of origin, x_2/m has integer values for transversal locations of the moving probe directly behind one of the zither wires. It is observed that $\bar{U}$ reaches a minimum behind a wire and a maximum halfway between two wires, which is consistent with ordinary wake measurements. Similarly, $\bar{V}$ vanishes directly behind a wire and halfway between two wires, as expected from symmetry. Even close to the zither ($x_1/d = 200$), the mean velocity $\bar{U}$ is within $\pm 2\,\%$ of the averaged free-stream velocity $\bar{U}_\infty$. This is similar to what was reported by Kellogg & Corrsin (1980), and can be attributed to a comparable incoming turbulence inducing the mixing of 'laminar' wakes downstream of the zither.

The behaviour of the r.m.s. values u' and v' presented in figure 3 is similar to that in a classical turbulent-wake profile except that the r.m.s. defect in the centre of the wakes is larger than it would be for a single wake. This could be due to the fact that the closest x_1 location (corresponding to 15 mm) is far enough from the zither to be strongly affected by background turbulence.

The Reynolds stress $\overline{uv}$ shown in figure 4 also has a nearly sinusoidal x_2 variation, with zero values approximately directly behind and halfway in between zither wires. Its decay with increasing downstream distance x_1 from the zither is very rapid, corresponding to a simultaneous mean-gradient $\partial\bar{U}/\partial x_2$ decay, and at $x_1/d = 600$, $\overline{uv}$ can be considered to be zero. The value of $\overline{uv}$ at $x_1/d = 200$ is of the same order of magnitude as u'^2 and v'^2.

The measured variation of the first- and second-order moments is in good qualitative agreement with earlier results of Townsend (1949) for a single fully turbulent wake.

The transversal correlations are shown in figures 5–7 for a range of transversal separations r_2 covering 6 mesh lengths. The maximum separation r_2 between probes was one grid mesh size M. The first subscript refers to the fixed probe and the second one to the moving probe. Since the flow is found to be non-homogeneous, correlations R_{12} and R_{21} are different in amplitude and phase. Both R_{11} and R_{22} show periodic oscillations with a period consistently equal to m. At $x_1/d = 200$ the oscillations have very large amplitudes, which in some cases reach negative values. For all downstream

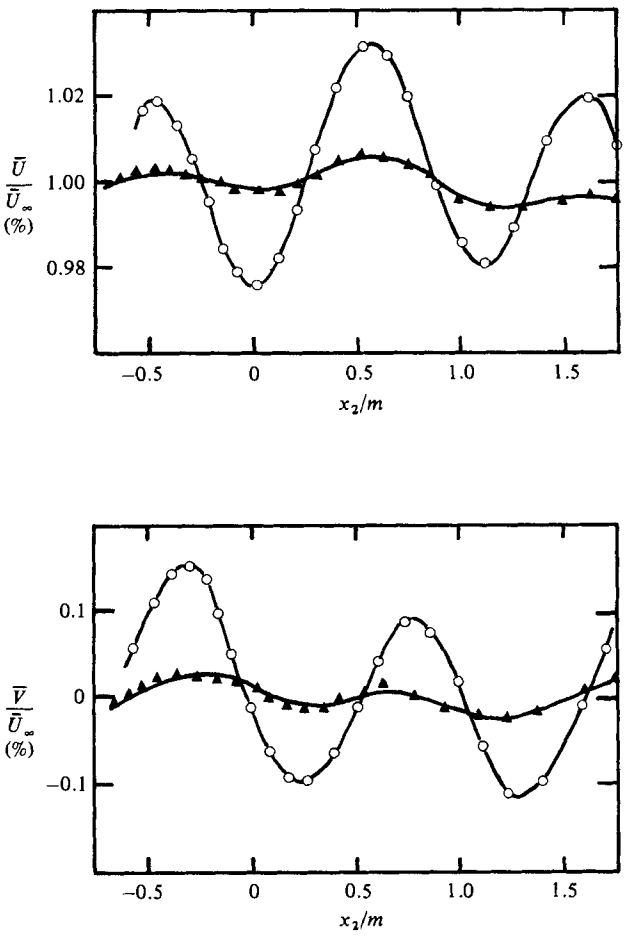

FIGURE 2. Mean velocities $\bar{U}/\bar{U}_\infty$ and $\bar{V}/\bar{U}_\infty$ versus x_2/m at $x_1/d = 200$ (○); 200 (▲).

locations x_1 the local maxima of $R_{22}(r_2)$ are shifted by a variable amount compared with locations corresponding to an integer value of r_2/m. Consideration of the mean profile $\bar{U}/\bar{U}_\infty$ shows that these maxima occur when the moving probe is directly behind a zither wire. So far we have found no satisfactory explanation for this result. As a reference, for homogeneous and isotropic turbulence, the correlations $R_{22}(r_2)$ and $R_{11}(r_2)$ are usually referred to as $f(r)$ and $g(r)$ respectively (e.g. Batchelor 1953).

Spatial–temporal correlations of the type $R_{ij}(r_2, \tau)$ have been computed from the measured time series for $x_1/d = 200$, 400 and 600. When compared with nearly isotropic turbulence correlations, these measurements exhibit a much slower decay time, up to 15 ms for $R_{11}(r_2, \tau)$ when r_2 approaches zero, compared with 0.7 ms for the data of Chen (1969). Thus the energy input in the transversal direction strongly affects the time decay of the correlations. This large degree of apparent stretching of the large scales in the main-flow direction is surprising, since the wire wakes, while very coherent, are so small.

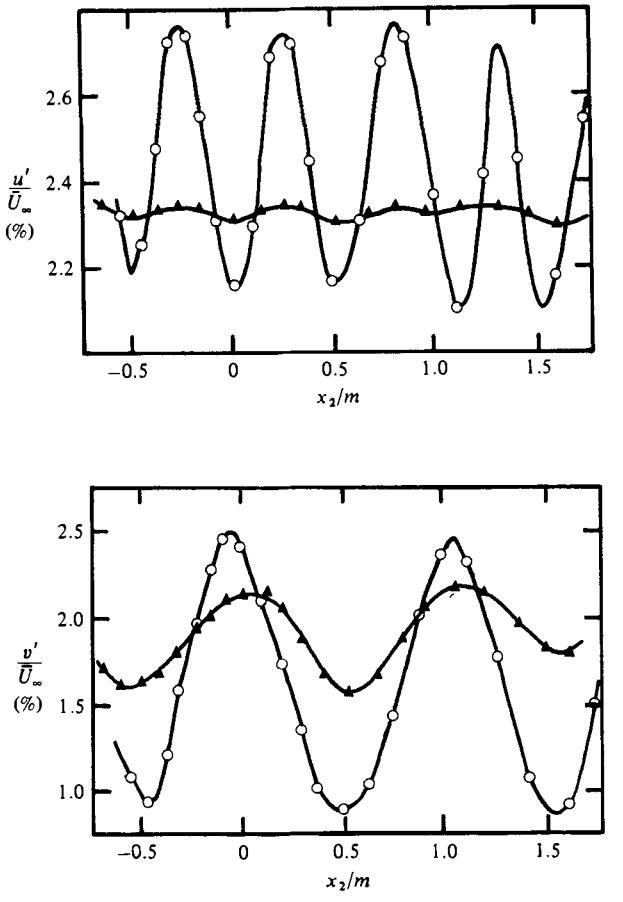

FIGURE 3. Turbulent intensities $u'/\bar{U}_\infty$ and $v'/\bar{U}_\infty$ versus x_2/m at $x_1/d = 200$ (○); 400 (▲).

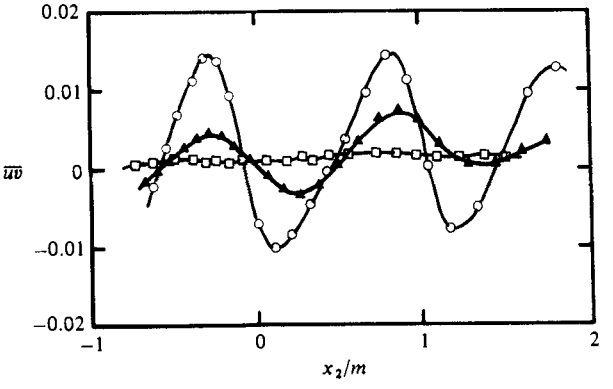

FIGURE 4. Reynolds stress $\overline{uv}$ versus x_2/m at $x_1/d = 200$ (○); 400 (▲); 600 (□).

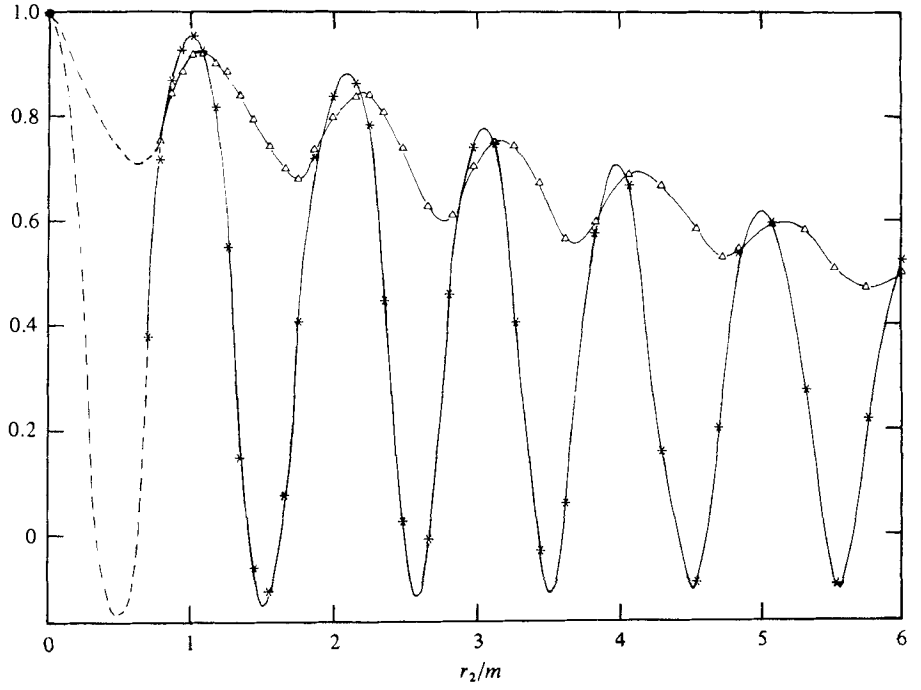

FIGURE 5. R_{11} (*) and R_{22} (△) versus r_2/m at $x_1/d = 200$.

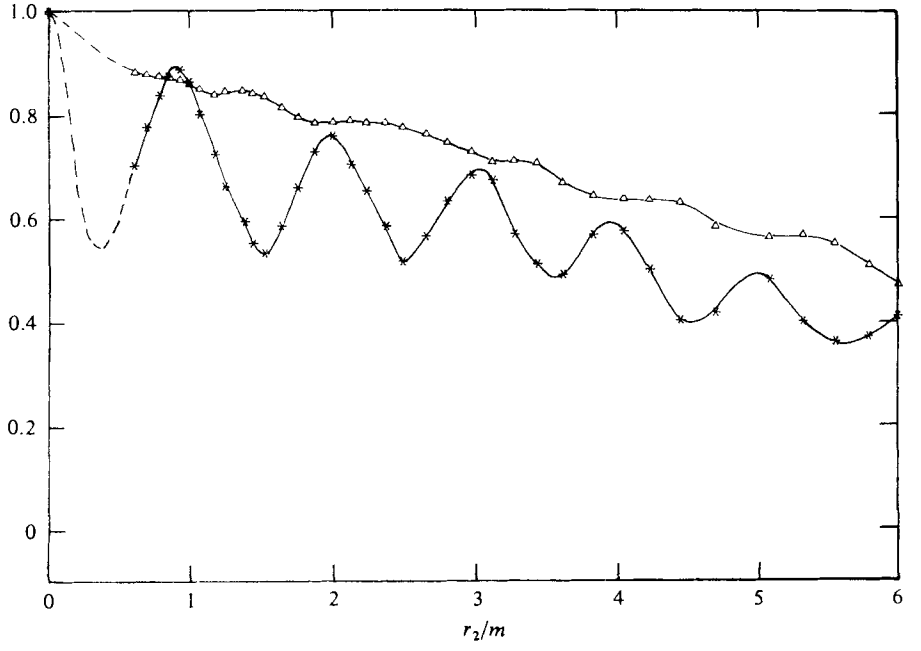

FIGURE 6. R_{11} (*) and R_{22} (△) versus r_2/m at $x_1/d = 400$.

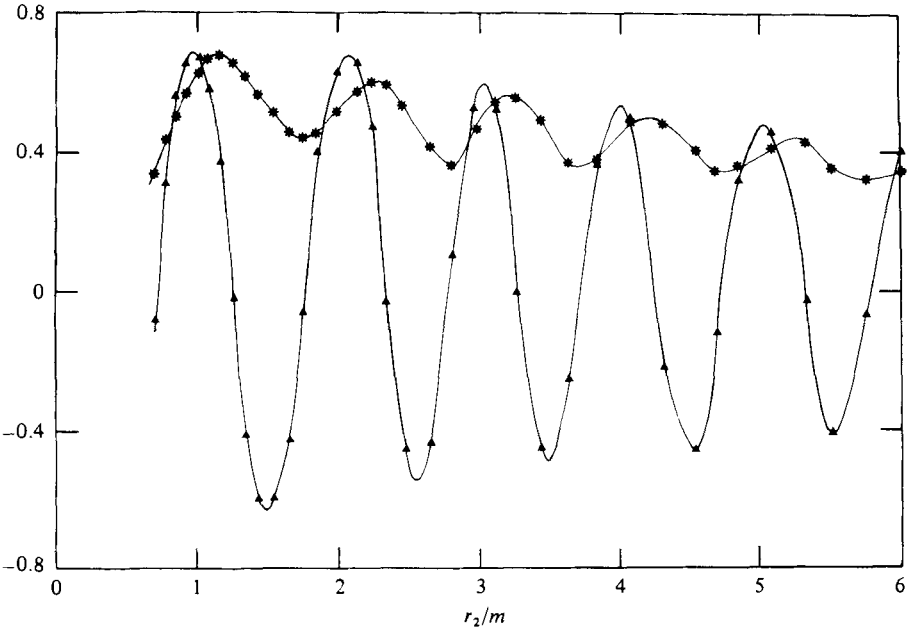

FIGURE 7. R_{12} (*) and R_{21} (▲) versus r_2/m at $x_1/d = 200$.

5. Spectral representation of the turbulence

The discrete Fourier transform of a discrete time series $u(T)$ ($T = 1, \ldots, N$) is defined as

$$F_u(\lambda) = \Delta T \sum_{T=1}^{N} u(T)\, e^{-2\pi i \lambda T} \quad (\lambda = 1, \ldots, \tfrac{1}{2}(N+1)),$$

where ΔT is the time interval between two consecutive samples. It follows that the one-dimensional power spectrum of $u(T)$ is

$$E_{11}(\lambda) = |F_u(\lambda)|^2,$$

and the cross-spectrum between two time series $u(T)$ and $v(T)$ is

$$E_{12}(\lambda) = F_u(\lambda)\, F_v^*(\lambda).$$

The real part is defined as the cospectrum and the imaginary part as the quadspectrum. It is possible to define two other quantities reflecting correlation and phase of the two signals in frequency or wavenumber space. The coherence is

$$\text{coh}\,(u, v) = \{[\text{Re}\,(E_{12})]^2 + [\text{Im}\,(E_{12})]^2\}^{\frac{1}{2}},$$

and the phase is

$$\text{phase}\,(u, v) = \tan^{-1} \frac{\text{Im}\,(E_{12})}{\text{Re}\,(E_{12})}.$$

For each velocity component, the power spectra at the various x_1/d locations are plotted on the same figure (figures 8 and 9 for E_{11} and E_{22} respectively) in order to emphasize the differences in shape occurring in the midfrequencies, i.e. between 10 and 1000 Hz. With $\bar{U}_\infty = 6.5$ m/s, the scaling factor $2\pi/\bar{U}_\infty$ to convert frequency to

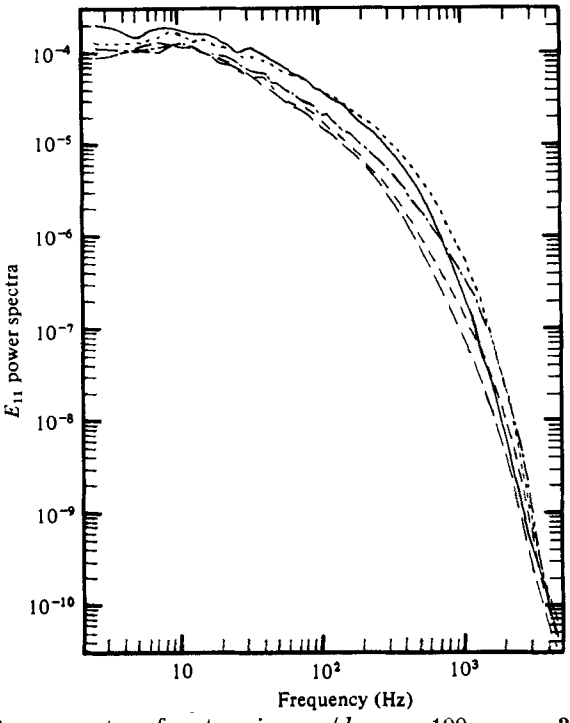

FIGURE 8. Power spectra of u at various x_1/d: ——, 100; . . . . ., 300; —·—·—, 600; – – – –, 1000; — — —, 1500.

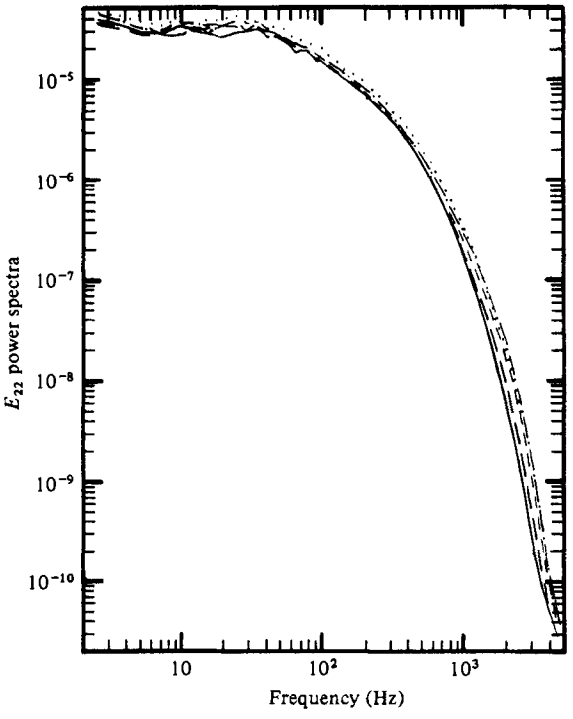

FIGURE 9. Power spectra of v at various x_1/d: ——, 100; . . . . ., 300; —·—·—, 600; – – – – –, 1000; — — —, 1500.

wavenumber k_1 is 0.967. This value is close enough to 1 to allow the frequency scales to be read directly as wavenumber scales as well.

As x_1 increases, there is a short growth period close to the zither up to $x_1/d = 300$, or equivalently $x_1/M = 0.45$. For the u-component there is evidence of strong energy transfer from the inertial range to the viscous range, while all frequencies below 600 Hz lose energy. For $x_1/d > 600$ the process is reversed, maintaining a nearly constant energy at the lower frequencies while losing energy at the higher frequencies. For $x_1/d > 1200$ the u-spectrum appears to reach a more self-similar decay regime, as observed for isotropic turbulence. This behaviour is in good agreement with that reported by Kellogg & Corrsin (1980), as shown in figure 8.

The shape of the v-spectrum (figure 9) appears to be relatively weakly affected by the disturbance, and at all downstream locations does not exhibit very sharp breaks in the spectral shape, as does that of u. However, when compared with isotropic turbulence, the v power spectrum has a reduced energy close to the zither and progressively regains energy to reach a nearly isotropic level eventually.

The cospectra and quadspectra of u and v are presented in figure 10. For an ideally isotropic turbulent flow, these quantities as well as the coherence and phase would be identically zero. The cospectra levels approach zero very rapidly after the initial growth period ends ($x_1/d > 200$). In the initial growth range, where there is production of Reynolds stress, most of the energy is contained in the midfrequencies between 10 and 800 Hz. The quadspectra are small compared with the cospectra: apparent 'fluctuations' in both parts of the cross-spectra are statistical errors due to the limited number of records used to estimate them.

The behaviour of the coherence (Itsweire 1983), which is a frequency-dependent cross-correlation, shows that the zither, in spite of its very low solidity and small mesh size, enhances the correlation between u and v even at the largest scales. This coherence disappears quickly when the Reynolds stress produced by the local transversal velocity gradients has decayed.

In order to compare the power spectra of u and v with the corresponding spectra for isotropic turbulence, the rate of dissipation of turbulent energy $\bar{\epsilon}$ was estimated using the isotropic formula

$$\bar{\epsilon} \approx \nu \left\{ 10 \overline{\left(\frac{\partial u}{\partial x_1}\right)^2} + \frac{5}{2} \overline{\left(\frac{\partial v}{\partial x_1}\right)^2} \right\}.$$

The terms on the right-hand side can be expressed as functions of the one-dimensional power spectra $E_{11}(k_1)$ and $E_{22}(k_1)$ respectively, e.g.

$$\overline{\left(\frac{\partial u}{\partial x_1}\right)^2} = \left(\frac{2\pi}{\overline{U}_\infty}\right)^2 \int_{-\infty}^{\infty} f^3 E_{11}(f)\, \mathrm{d}(\log f).$$

Figure 11 shows self-preserving plots of the velocity-gradient spectra for $x_1/d = 100$ and 1500. Close to the zither, the contribution of v to the total dissipation rate is much smaller than farther downstream, where the turbulence is nearly isotropic. The dissipation rates for various x_1/d are shown in table 3. For small x_1/d the values are higher than the dissipation rate of the incoming turbulence $\bar{\epsilon} \approx 760$ cm/s presented in table 3, indicating an increased energy cascade from the inertial range to the viscous range.

Some of the power spectra are plotted in figure 12 (a, b) in dimensionless form using Kolmogorov length and velocity scales $\eta = (\nu^3/\epsilon)^{\frac{1}{4}}$ and $v_k = (\epsilon\nu)^{\frac{1}{4}}$ respectively. The spectra are compared with nearly isotropic spectra from Helland *et al.* (1979), for which the mean speed and turbulent r.m.s. velocities were 10 % higher than for the

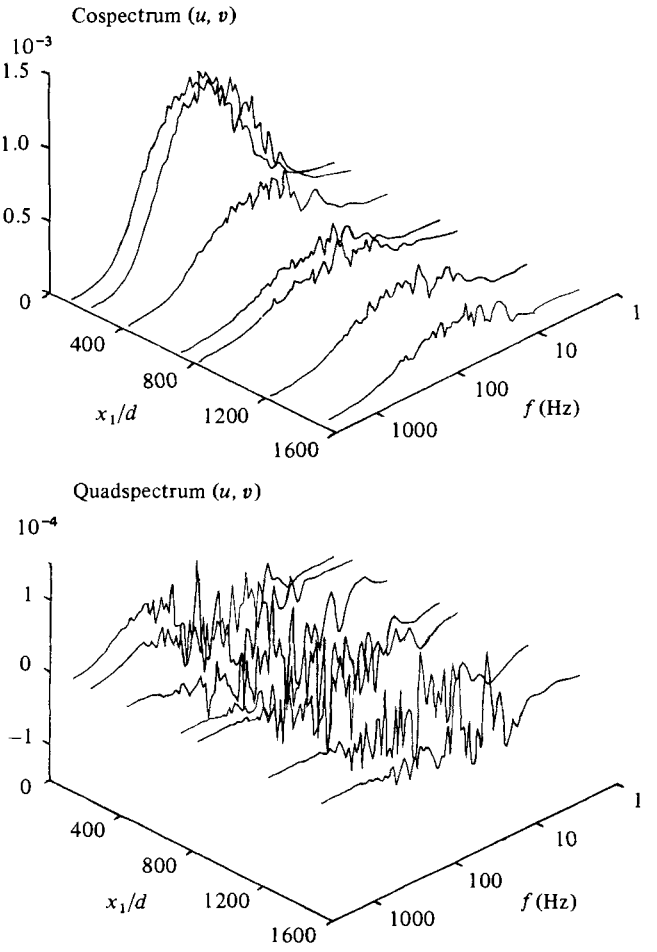

FIGURE 10. Co- and quadspectra of u and v at x_1/d = 100, 200, 400, 700, 800, 1200 and 1500.

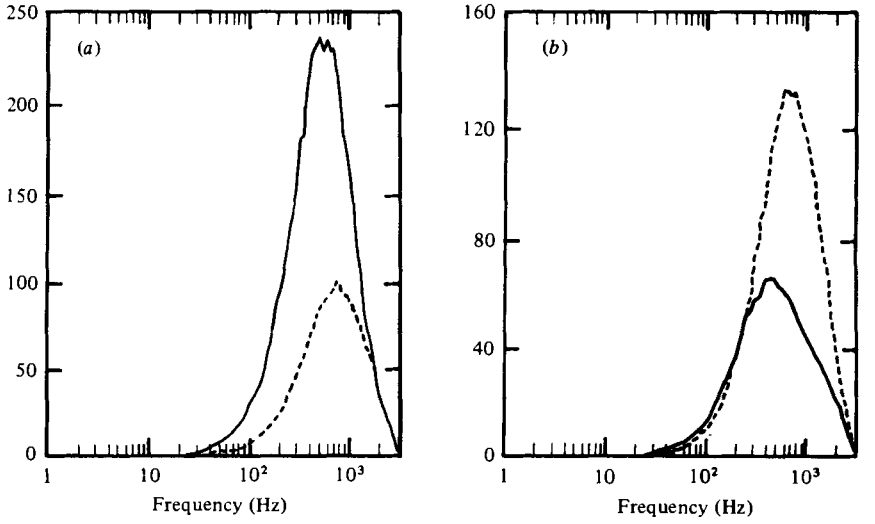

FIGURE 11. Self-preserving plots of the velocity-gradient spectra; ——, $\partial u/\partial x$; – – – –, $\partial v/\partial x$. (a) x_1/d = 100; (b) x_1/d = 1500.

x_1/d	Dissipation rate $\bar{\epsilon}$ (cm^2/s^3)
100	1380
200	1796
400	1690
700	1124
800	945
1200	688
1500	584

TABLE 3. Dissipation rates $\bar{\epsilon}$ as function of downstream distance from the zither

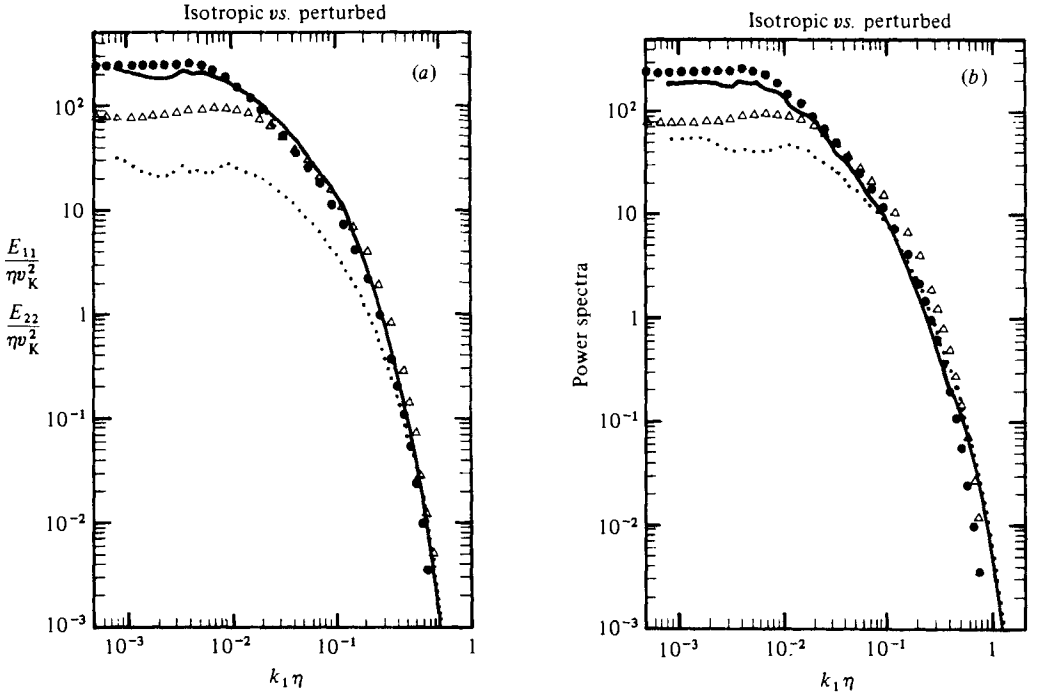

FIGURE 12. Normalized velocity power spectra of u and v at $x_1/d = 100$ (*a*) and 800 (*b*) compared with isotropic spectra. Present results: ——, u; . . . ., v. From Helland *et al.* (1979): ●●●, u; △△△, v.

zither case. This difference accounts for the slightly higher spectral levels at low wavenumbers.

In contrast with the nearly isotropic spectra, the zither v-component power-spectral levels do not cross over the u-spectra when $x_1/d < 800$, and they have a smaller slope than the isotropic spectra for scales larger than the viscous scales ($> 10\eta$). For $x_1/d = 200$, 400 and 800 there is a short range of -1 slope in the v-spectra (Itsweire 1983). At $x_1/d = 1500$ both spectra, especially E_{11}, are closely locally isotropic, except for the smallest viscous scales, which contain more energy. This excess energy is similar to Townsend's (1951) results. In his work, Townsend modelled the local inhomogeneities of the flow in terms of a random distribution of vortex lines and thin vortex sheets.

6. Bispectral computations and one-dimensional energy transfer

With the previous definition of the discrete fast Fourier transform, Helland *et al.* (1979) defined several experimentally measureable bispectra such as

$$B_{uuu}(\lambda_1, \lambda_2) = \langle F_u(\lambda_1) F_u(\lambda_2) F_u^*(-\lambda_1 - \lambda_2) \rangle,$$

where $\langle\ \rangle$ denotes a statistical average and F_u the discrete FFT of u. The bispectra can also be transformed from the frequency domain to the wavenumber domain by multiplying frequencies by the scaling factor of $2\pi/U_\infty$ using Taylor's hypothesis $x_1 = -U_\infty t$. The cross-bispectra and their variances were computed using the algorithm proposed by Lii & Helland (1981). This algorithm divides the frequency domain into averaging rectangles that help reduce the variance of the bispectral estimates. This is crucial for cross-bispectra, since, like high-order cross-moments, their amplitude is less than for single-channel bispectra. In the present study the averaging rectangles were 50 Hz × 50 Hz.

Two bispectra were computed, B_{uuu} and B_{vuv}, corresponding to the one-dimensional contributions of two of the inertial terms $\overline{uu\,\partial u/\partial x_1}$ and $\overline{uv\,\partial v/\partial x_1}$ in the equations for the evolution of $\overline{u^2}$ and $\overline{v^2}$ downstream of the wire wake region (other important terms are explicitly mentioned in §7):

$$\overline{U}\frac{\partial}{\partial x_1}\left(\frac{\overline{u^2}}{2}\right) = \overline{-u^2\frac{\partial u}{\partial x_1}} - \overline{uv\frac{\partial u}{\partial x_2}} + \ldots + \nu\overline{u\nabla^2 u},$$

$$\overline{U}\frac{\partial}{\partial x_1}\left(\frac{\overline{v^2}}{2}\right) = \overline{-uv\frac{\partial v}{\partial x_1}} - \overline{v^2\frac{\partial v}{\partial x_2}} + \ldots + \nu\overline{v\nabla^2 v}.$$

No attempt was made to compute B_{vvv} because of the low resolvability of this bispectrum, as pointed out by Helland *et al.* (1979). Resolvability tables for the computed bispectra are presented in Appendix A of Itsweire (1983). The resolvabilities are consistent with previous measurements done in the AMES wind tunnel.

The real part of B_{uuu} was never well resolved, except for the frequencies below 500 Hz. For fully isotropic turbulence the real part of B_{uuu} would be identically zero (e.g. Helland *et al.* 1979), and the observed non-zero values may be a manifestation of the anisotropy introduced by the zither. Perspective views of the real part of B_{uuu} (Itsweire 1983) also show that for $x_1/d = 100$–400 the bispectrum is essentially a positive broad peak with two additional lobes. For $x_1/d > 700$ the peak is mostly negative and narrower, in agreement with measurements by Lii *et al.* (1982).

The imaginary part of B_{uuu} is well resolved for almost all frequency pairs. The rounded ratios of the bispectral estimates to the standard deviations of the estimates was greater than 6 in all regions of significant bispectra (for complete tables see Itsweire 1983). Compared with the isotropic case of Helland *et al.* (1979), for $x_1/d \leqslant 400$ the imaginary parts of B_{uuu} have additional negative lobes around the positive spike at the low-frequency corners, apparently a combined effect of the local anisotropy and the initial growth period close behind the zither. Farther downstream ($x_1/d \geqslant 700$) the imaginary parts of B_{uuu} have the same shape and magnitude as in the isotropic case. B_{vuv} exhibits behaviour similar to B_{uuu}. The real part is not resolvable while the imaginary part is (Itsweire 1983).

All bispectral estimates can be used to generate one-dimensional transfer terms, according to the approach outlined by Wilson (1974) and adapted by Van Atta (1979*a*). The method is suitable for this particular experiment, since the method

involves a Fourier decomposition of the velocity field in which the disturbance introduced by the zither can be represented ideally as a single Fourier mode which is orthogonal to the x_1 direction along which the transfer terms are measured.

A Fourier decomposition of the x_1 and x_2 momentum equations gives the rate of change of the r.m.s. velocities for the ith Fourier mode u_i as:

$$\overline{U}\frac{\partial}{\partial x_1}\left(\frac{\overline{u_i^2}}{2}\right) = -\overline{u_i \sum_k U_k \frac{\partial}{\partial x_1}(\sum_l u_l)} + \ldots + \overline{\nu u_i \nabla^2(\sum_k u_k)},$$

where the total velocity component u is

$$u(x_1) = \sum_k u_k = \sum_k \frac{C_k}{k} \sin(kx_1 + \theta_k).$$

The term of present interest is the first term on the right-hand side, i.e. the inertial transfer term. It is a measure of the energy transfer between the frequency l and any other frequency k associated with a wavenumber in the longitudinal direction. The last term describes the rate of loss of downstream (x_1) energy due to viscous dissipation and viscous transport. Similarly, for the x_2 component v, the equation is

$$\overline{U}\frac{\partial}{\partial x_1}\left(\frac{\overline{v_i^2}}{2}\right) = -\overline{v_i \sum_k u_k \frac{\partial}{\partial x_1}(\sum_l v_l)} + \ldots + \overline{\nu v_i \nabla^2(\sum_k v_k)},$$

where the total velocity component v is

$$v(x_1) = \sum_k v_k = \sum_k \frac{C'_k}{k} \sin(kx_1 + \theta'_k).$$

Again, the first term on the right-hand side describes the energy transfer between frequencies l and k, while the last term describes the rate of loss of transversal (x_2) energy at frequency l due to viscosity and viscous transport.

The Fourier decomposition of the velocity field is subject to the condition that the inertial terms arise only from three types of interactions, called 1, 2 and 3 by Wilson:

1. $\dfrac{-C_l C_m C_k}{4lm} \cos(\theta_l - \theta_m + \theta_k)$ for $l - m + k = 0$,

2. $\dfrac{-C_l C_m C_k}{4lm} \cos(\theta_l - \theta_m - \theta_k)$ for $l - m - k = 0$,

3. $\dfrac{C_l C_m C_k}{4lm} \cos(\theta_l + \theta_m - \theta_k)$ for $l + m - k = 0$.

The three types of interactions do not have any particular physical meaning when taken separately, and need to be combined to obtain the net inertial energy transfer to and from any given frequency. These interactions are directly related to the imaginary part of the measured bispectra presented here, as shown by Van Atta (1979*a*). For any given frequency l all the bispectral values of the imaginary part corresponding to frequency pairs (k, m) satisfying any of the relationships imposed by the interactions of type 1, 2 or 3 are summed together. The result is $lS(l, k)$, which is the net energy transfer from frequency k to frequency l due to triadic interactions.

The results of some of these computations are plotted in figures 13 and 14. For each frequency k, the same vertical scale for $lS(l, k)$ has been chosen for the various x_1/d in order to compare the quantitative evolution of the one-dimensional energy

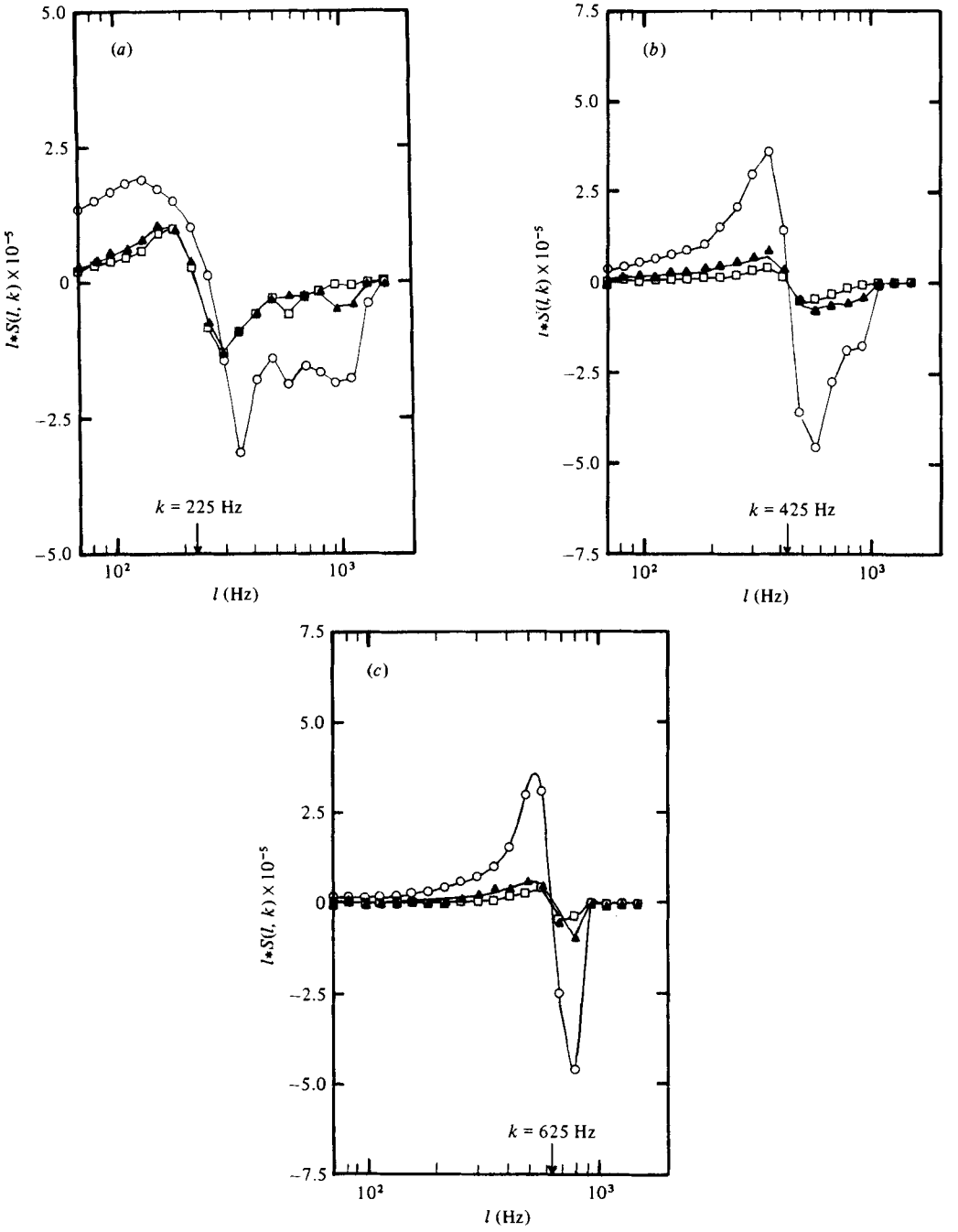

FIGURE 13. One-dimensional longitudinal energy transfer at $x_1/d = 200$ (○), 700 (▲) and 1500 (□) for $k = 225$ Hz (*a*), 425 Hz (*b*) and 625 Hz (*c*).

transfer. Positive values of $lS(l, k)$ indicate a net transfer from l to k, while negative values show a net loss of energy from k to l.

The first transfer term computed from B_{uuu} shows that, as expected, the zither increases the amount of energy transferred and broadens the range of frequencies involved in this exchange as compared with the isotropic case. An increased energy

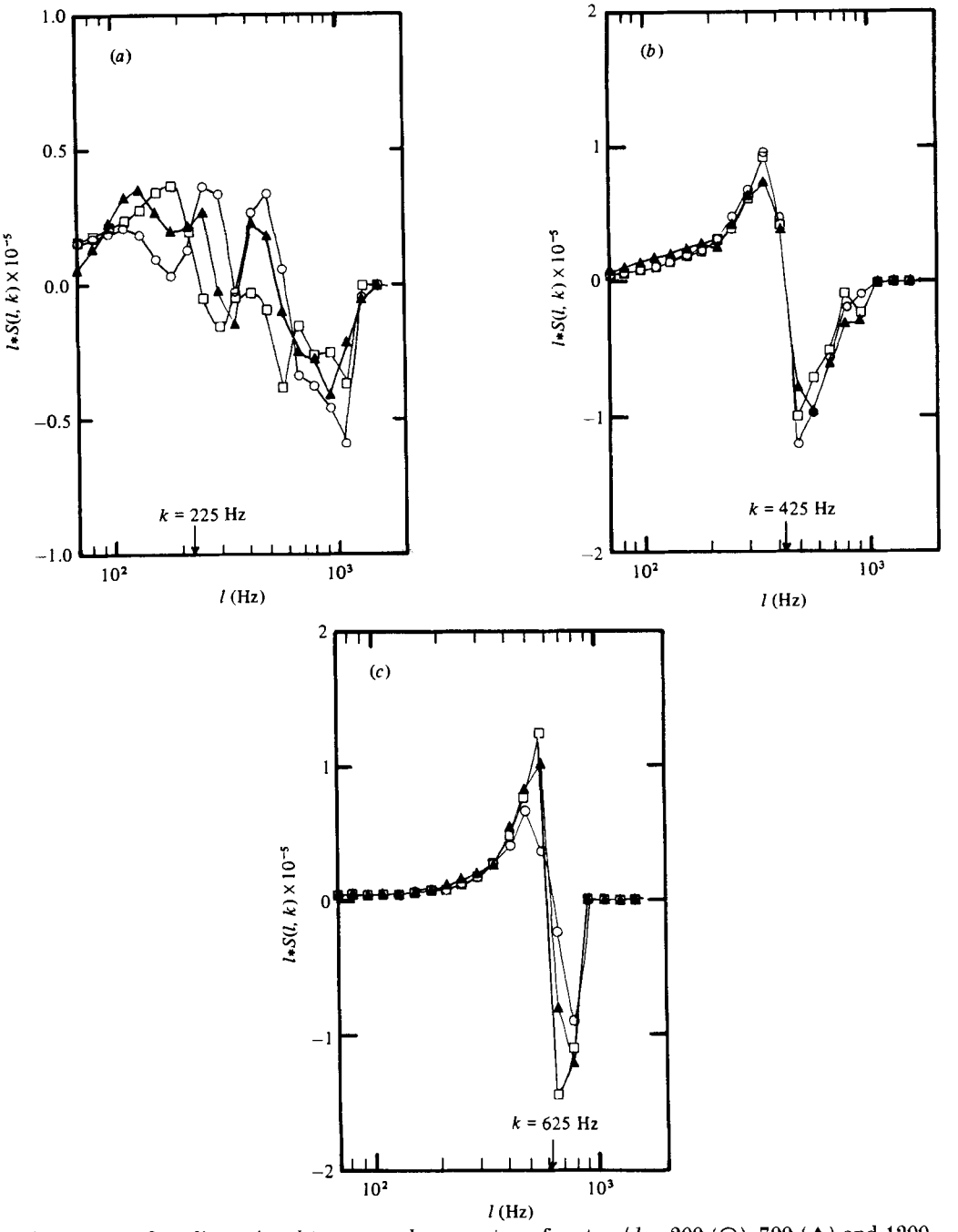

FIGURE 14. One-dimensional transversal energy transfer at $x_1/d = 200$ (○), 700 (▲) and 1200 (□) for $k = 225$ Hz (*a*), 425 Hz (*b*) and 625 Hz (*c*).

transfer due to the initial growth of the disturbance occurs only at the highest frequencies, which is consistent with the power-spectrum results and observations made previously.

The second transfer term, corresponding to B_{vuv}, does not change as systematically or dramatically as that for B_{uuu} when moving farther downstream. This is surprising,

since the imaginary part of the bispectra B_{vuv} exhibits differences in level and shape for different stations x_1/d. This insensitivity is undoubtedly connected with the fact that the spectrum of the velocity fluctuation v (figure 9) is not affected by the zither as strongly as that of u. The imaginary parts of the bispectra corresponding to figure 13(*a*) were not resolved well enough at the lower frequencies to give a good estimate of these transfer terms.

7. Energy budget and return to isotropy

Now consider the evolution equations for the r.m.s. turbulent velocities and the Reynolds stress which are derived from the Navier–Stokes equations for an incompressible fluid (e.g. Townsend 1956). We assume that the initial turbulent field is homogeneous and isotropic and that the effect of the zither on the mean velocity is essentially limited to the (x_2, x_3)-plane, i.e. all the gradients of mean velocity in the x_1 direction are considered to be negligible. Furthermore, the flow is statistically steady in time, i.e. $\partial(\overline{\ })/\partial t = 0$. The equation for the evolution of $\overline{u^2}$ (e.g. Townsend 1956) is

$$\underset{(1)}{\overline{U}\frac{\partial \overline{u^2}}{\partial x_1}} = \underset{(2)}{-2\overline{u^2}\frac{\partial \overline{U}}{\partial x_1}} \underset{(3)}{-2\overline{uv}\frac{\partial \overline{U}}{\partial x_2}} \underset{(4)}{-\frac{\partial \overline{u^3}}{\partial x_1}} \underset{(5)}{-\frac{\partial \overline{u^2 v}}{\partial x_2}} \underset{(6)}{-\frac{2}{\rho}\overline{u\frac{\partial p}{\partial x_1}}} + \underset{(7)}{\nu\overline{u\frac{\partial^2 u}{\partial x_k \partial x_k}}}.$$

The transversal gradients are larger than the longitudinal gradients, since the characteristic length in the x_1 direction is of order M, as compared with m for the transversal direction x_2. Therefore (2) can be neglected compared with (3), and (4) can be neglected compared with (5). The total turbulent-energy dissipation rate to which (7) contributes is (see table 2) at least an order of magnitude smaller than (1) (0.2 compared with 10 m^2/s^3). The energy balance reduces to terms (1) on the left-hand side and (3), (5) and (6) on the right-hand side. The pressure–velocity correlation, which is the only term that cannot be measured directly, can be estimated from the evolution equations.

Kellogg & Corrsin (1980) considered only the balance between terms (1) and (3), and represented Reynolds stress and mean and r.m.s. velocities as sinusoidal functions of x_2 to get an averaged energy-growth estimate. At $x_1/d = 200$ they found

$$\frac{\overline{(u^2)}_{\mathrm{av}}}{\overline{(u^2)}_0} \approx 1.8.$$

Their measured value was 2.7. In the present experiment, which had slightly different experimental conditions, the measured ratio is 2.26. Figures 15 and 16 show the first two terms (1) and (3) for $x_1/d = 200$ and 400. The sum of these two curves is a non-zero, positive spatially oscillating function. The positive value is consistent with the low estimate of Kellogg & Corrsin for the energy amplification by the zither. Figure 17 shows the estimates of the pressure–velocity correlation term for $x_1/d = 200$, 400 and 600. Many more data points in both x_1 and x_2 would be needed to get a tighter estimate of this term but, in any case, the term is not negligible. For a single turbulent wake, Townsend's (1949) estimate of the pressure–velocity correlation has a zero mean value when averaged along the wake. This result suggests that for small downstream distances x_1/d from the zither, the lateral flapping of the wakes caused by the incoming turbulence may be the mechanism responsible for producing a non-zero pressure–velocity correlation.

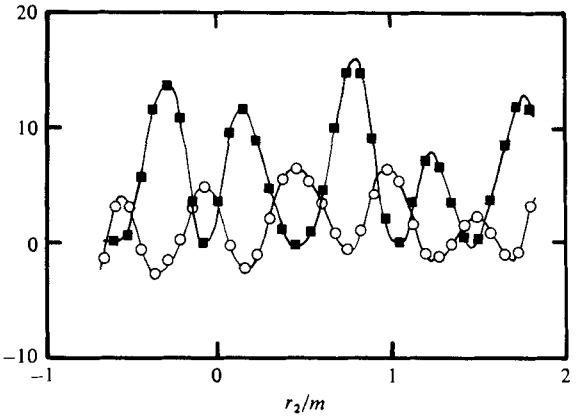

FIGURE 15. Energy balance for the evolution of u at $x_1/d = 200$. -○-○-, $\overline{U}\,\partial\overline{u^2}/\partial x_1$; -■-■-, $2\overline{uv}\,\partial\overline{U}/\partial x_2$.

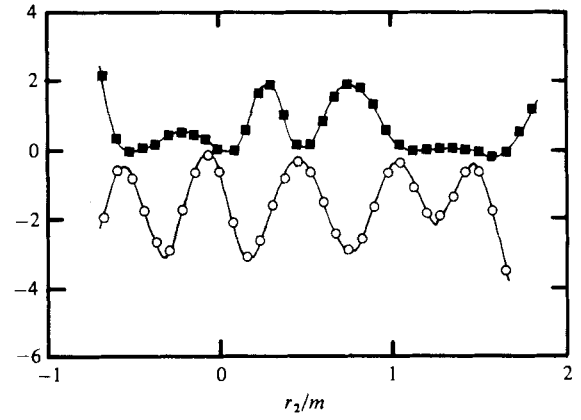

FIGURE 16. Energy balance for the evolution of u at $x_1/d = 400$: ○—○, $\overline{U}\,\partial\overline{u^2}/\partial x_1$; -■-■-, $2\overline{uv}\,\partial\overline{U}/\partial x_2$.

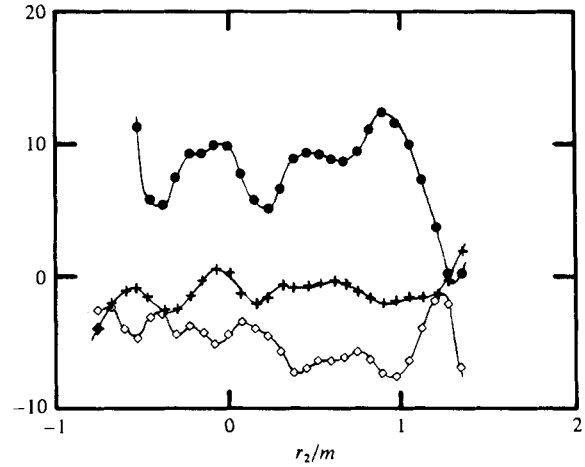

FIGURE 17. Estimate of the pressure–velocity correlation $-(2/\rho)\,\overline{u\,\partial p/\partial x_1}$ at $x_1/d = 200$ (●); 400 (+); 600 (◇).

With arguments similar to those for the previous equation, the equation for the evolution of $\overline{uv}$ can be simplified as follows:

$$\underset{(1)}{\overline{U}\frac{\partial \overline{uv}}{\partial x_1}} = \underset{(2)}{-\overline{v^2}\frac{\partial \overline{U}}{\partial x_2}} \underset{(3)}{-\frac{\partial \overline{uv^2}}{\partial x_2}} \underset{(4)}{-\frac{1}{\rho}\overline{\left(v\frac{\partial p}{\partial x_1}+u\frac{\partial p}{\partial x_2}\right)}}.$$

Both terms (1) and (2) are zero for the incoming turbulence. Figures 18 and 19 show that the terms (1) and (2) are nearly in balance at $x_1/d = 200$ and 400 respectively. This balance provides support for the generating mechanism of the Reynolds stress proposed by Kellogg & Corrsin, who suggested that the lateral velocity flopping the wakes was nearly v, creating a longitudinal fluctuation u equal to

$$u \sim -v\frac{\partial \overline{U}}{\partial x_2}.$$

As expected, the estimated pressure–velocity correlation term shown in figure 20 does not produce any mean contribution in the energy balance, when averaged in the x_2 direction.

As mentioned in §5, the relaxation of the perturbed turbulence is very fast. Kellogg & Corrsin found the decay to be exponential, in good agreement with the Kraichnan (1959) prediction. Figure 21 shows that the dissipation rate $\bar{\epsilon}$ decays like $(x_1)^{-0.8}$ for $x_1/d > 400$. The final turbulent intensity levels u' and v' are reduced, as predicted by Townsend (1951). Townsend used various wire gauzes behind a classical biplane grid, which produced a u' level lower than the v' level far downstream from his wire gauzes. This latter effect is not observed in the present experiment because of the much lower zither solidity and smaller wires.

8. Conclusions and future prospects

Two main phases in the decay of the disturbance are observed. For short distances from the zither, $x_1/d < 300$, a growth period is observed, characterized by increasing dissipation rate and longitudinal turbulence intensity. Over this range of x_1/d there is also production of shear stress $\overline{uv}$ from the local mean gradients of the interacting wakes of the zither wires, which complicates the nature of the disturbance. Overall, the zither seems to stretch even the large scales along the longitudinal axis by a combined action of the mean shears of opposite sign in neighbouring wakes. This result is somewhat surprising, since the scale of the shear is in the viscous range.

When the Reynolds stress and the mean shears have vanished, the return to isotropy starts. The rapid decay of the r.m.s. velocity u between $x_1/d = 300$ and 800 corresponds to a rapid loss of energy in the longitudinal power spectrum. A possible explanation for this phenomenon would be a relaxation of the large scales to a more isotropic form. Farther downstream, these large eddies will retain some anisotropy, since they will only interact weakly with the remaining turbulence; then only the smallest scales are losing energy owing to viscous dissipation. These interpretations are consistent with observations that the transversal component is gaining some energy at the largest scales. For $x_1/d > 1200$ the turbulence reaches its final period of decay.

Comparison between the present experimental results and available theoretical predictions is very difficult for several reasons. The separation between the perturbation scale and the turbulence scales was small, much smaller than in the theory. The amount of energy introduced by the zither was not negligible and was distributed

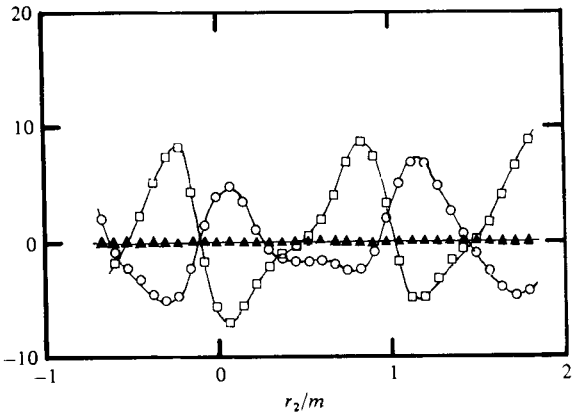

FIGURE 18. Energy balance for the evolution of $\overline{uv}$ at $x_1/d = 200$: ○, $\overline{U}\,\partial\overline{uv}/\partial x_1$; ▲, $\overline{uv}\,\partial\overline{U}/\partial x_1$; □, $\overline{v^2}\,\partial\overline{U}/\partial x_2$.

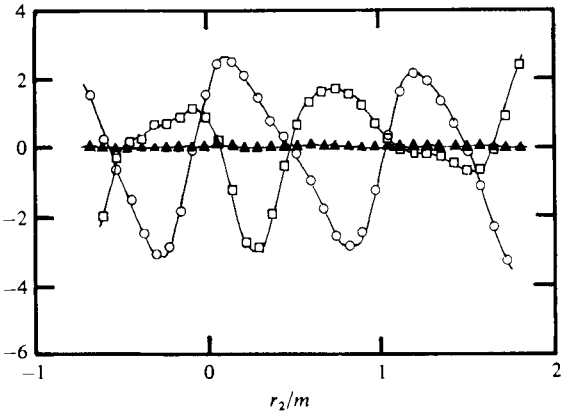

FIGURE 19. Energy balance for the evolution of uv at $x_1/d = 400$: ○, $\overline{U}\,\partial\overline{uv}/\partial x_1$; ▲, $\overline{uv}\,\partial\overline{U}/\partial x_1$; □, $\overline{v^2}\,\partial\overline{U}/\partial x_2$.

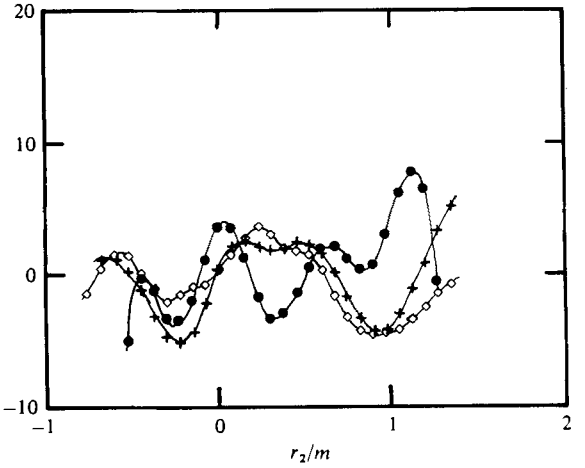

FIGURE 20. Estimate of pressure–velocity correlation $-(1/\rho)\,(\overline{v\,\partial p/\partial x_1} + \overline{u\,\partial p/\partial x_2})$ at $x_1/d = 200$ (●); 400 (+); 600 (◇).

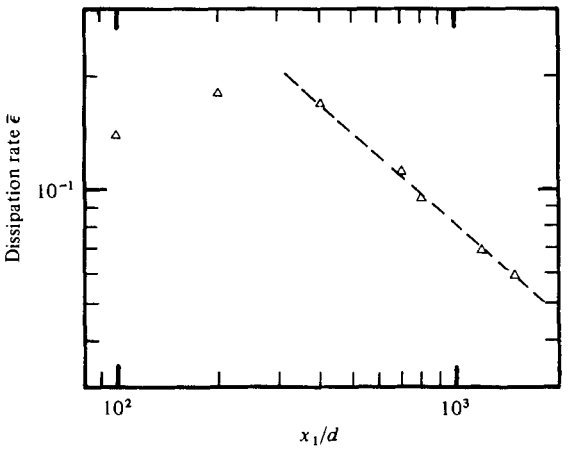

FIGURE 21. Dissipation rate versus x_1/d.

in a narrow plane slab instead of the ideal spherical shell in wavenumber space of the theories. Kellogg & Corrsin (1980) could only compare the decay of the amplitude of the first perturbation cycle of the correlation $R(r)$ to Kraichnan's (1959) linear estimate for a small perturbation at high wavenumber. This result does not provide imformation on the local redistribution of the perturbative energy.

Because of the complicated wake interactions, the representation of the zither disturbance as being simply spectrally local does not seem to be very appropriate. A more ideal experiment might introduce a similar perturbation in a scalar field, but fundamental difficulties arise when trying to introduce a scalar disturbance without a simultaneous velocity perturbation. This case would perhaps provide a better basis for comparison with direct numerical simulation, which can in principle approximate the perturbation as a single Fourier mode.

REFERENCES

BATCHELOR, G. K. 1953 *Theory of Homogeneous Turbulence*. Cambridge University Press.

CHEN, W. Y. 1969 Ph.D. thesis, University of California, San Diego.

COLLIS, D. C. & WILLIAMS, M. J. 1959 Two-dimensional convection from heated wires at low Reynolds numbers. *J. Fluid Mech.* **6**, 357–384.

HELLAND, K. N., LII, K. S. & ROSENBLATT, M. 1977 Bispectra of atmospheric and wind tunnel turbulence. In *Proc. Symp. on Applications of Statistics* (ed. P. R. Krishnaiah), pp. 223–248. North-Holland.

HELLAND, K. N., LII, K. S. & ROSENBLATT, M. 1979 Bispectra and energy transfer in grid-generated turbulence. In *Developments in Statistics* (ed. P. R. Krishnaiah), vol. 2, pp. 123–155. Academic.

HERRING, J. R. 1980 Theoretical calculations of turbulent bispectra. *J. Fluid Mech.* **97**, 193–204.

ITSWEIRE, E. C. 1983 An experimental study of the response of a nearly isotropic grid turbulence to a spectrally local disturbance. Ph.D. thesis, University of California, San Diego.

KELLOGG, R. M. 1965 Evolution of a spectrally local disturbance in a grid-generated turbulent flow. Ph.D. thesis, The John Hopkins University.

KELLOGG, R. M. & CORRSIN, S. 1980 Evolution of a spectrally local disturbance in grid-generated nearly isotropic turbulence. *J. Fluid Mech.* **96**, 641–669.

KRAICHNAN, R. H. 1959 The structure of isotropic turbulence at very high Reynolds numbers. *J. Fluid Mech.* **5**, 497–543.

LII, K. S. & HELLAND, K. N. 1981 Cross bispectrum computation and variance estimation. *ACM Trans. Math. Software* **7**, 284–294.

LII, K. S., ROSENBLATT, M. & VAN ATTA, C. W. 1976 Bispectral measurements in turbulence. *J. Fluid Mech.* **77**, 45–62.

SIRIVAT, A. & WARHAFT, Z. 1983 The effect of a passive cross-stream temperature gradient on the evolution of temperature variance and heat flux in grid turbulence. *J. Fluid Mech.* **128**, 323–346.

SREENIVASAN, K. R., TAVOULARIS, S., HENRY, R. & CORRSIN, S. 1980 Temperature fluctuations and scales in grid-generated turbulence. *J. Fluid Mech.* **99**, 545–573.

TOWNSEND, A. A. 1949 Fully developed turbulent wake of a circular cylinder. *Austral. J. Sci. Res.* A **2**, 451–468.

TOWNSEND, A. A. 1951 The passage of turbulence through wire gauzes. *Q. J. Mech. Appl. Maths* **4**, 308–320.

TOWNSEND, A. A. 1956 *The Structure of Turbulent Shear Flow.* Cambridge University Press.

VAN ATTA, C. W. 1979*a* Bispectral measurements in turbulence computations. In *Proc. 6th Intl Conf. on Numerical Methods in Fluid Dynamics, Tbilisi, June 1978* (ed. H. Cabannes, M. Holt & V. V. Rusanov). Lecture Notes in Physics, vol. 90, pp. 530–536. Springer.

VAN ATTA, C. W. 1979*b* Inertial range bispectra in turbulence. *Phys. Fluids* **22**, 1440–1442.

WARHAFT, Z. 1980 An experimental study of the effect of uniform strain on thermal fluctuations in grid generated turbulence. *J. Fluid Mech.* **99**, 545–573.

WARHAFT, Z. & LUMLEY, J. L. 1978 An experimental study of the decay of temperature fluctuations in grid-generated turbulence. *J. Fluid Mech.* **88**, 659–684.

WILSON, J. R. 1974 Ph.D. thesis, University of British Columbia.

YEH, T. T. & VAN ATTA, C. W. 1973 Spectral transfer of scalar and velocity fields in heated-grid turbulence. *J. Fluid Mech.* **58**, 233–261.